3D Graphene Fibers Grown by Thermal Chemical Vapor Deposition

Jie Zeng, Xixi Ji, Yihui Ma, Zhongxing Zhang, Shuguang Wang, Zhonghua Ren, Chunyi Zhi, and Jie Yu*

3D assembly of graphene sheets (GSs) is important for preserving the merits of the single-atomic-layered structure. Simultaneously, vertical growth of GSs has long been a challenge for thermal chemical vapor deposition (CVD). Here, vertical growth of the GSs is achieved in a thermal CVD reactor and a novel 3D graphene structure, 3D graphene fibers (3DGFs), is developed. The 3DGFs are prepared by carbonizing electrospun polyacrylonitrile fibers in NH_3 and subsequently in situ growing the radially oriented GSs using thermal CVD. The GSs on the 3DGFs are densely arranged and interconnected with the edges fully exposed on the surface, resulting in high performances in multiple aspects such as electrical conductivity (3.4×10^4– 1.2×10^5 S m^{-1}), electromagnetic shielding (60 932 dB cm^2 g^{-1}), and super-hydrophobicity and superoleophilicity, which are far superior to the existing 3D graphene materials. With the extraordinary properties along with the easy scalability of the simple thermal CVD, the novel 3DGFs are highly promising for many applications such as high-strength and conducting composites, flexible conductors, electromagnetic shielding, energy storage, catalysis, and separation and purification. Furthermore, this strategy can be widely used to grow the vertical GSs on many other substrates by thermal CVD.

Graphene possesses many extraordinary properties such as high electrical conductivity ($\approx 2.4 \times 10^5$ S m^{-1}),[1,2] thermal conductivity (≈ 5300 W m^{-1} K^{-1}),[3] charge carrier mobility ($\approx 2 \times 10^5$ cm^2 V^{-1} s^{-1}),[4,5] and specific surface area (SSA) (2630 m^2 g^{-1}),[6] generating many fascinating applications in the areas of electronic device,[6,7] energy storage,[8–10] catalysis,[11] electrical and thermal conducting composites,[12,13] and so forth. Nevertheless, these

J. Zeng, X. X. Ji, Y. H. Ma, Z. X. Zhang, S. G. Wang, Z. H. Ren, Prof. J. Yu
Shenzhen Engineering Lab for Supercapacitor Materials
Shenzhen Key Laboratory for Advanced Materials
Department of Material Science and Engineering
Shenzhen Graduate School
Harbin Institute of Technology
University Town
Shenzhen 518055, China
E-mail: jyu@hit.edu.cn
Prof. C. Y. Zhi
Department of Physics and Materials Science
City University of Hong Kong
Tat Chee Avenue, Kowloon, Hong Kong, China

The ORCID identification number(s) for the author(s) of this article can be found under https://doi.org/10.1002/adma.201705380.

excellent properties were obtained only on single crystal graphene. Practically, except for the application of electronic devices, graphene is generally used by assembling microscale sheets into macroscopic objects for most other applications, resulting in sharp decline of the properties due to stacking agglomeration and weak sheet-to-sheet bonding.[10]

A major route to coping with this problem is to prepare 3D graphene network, in which the graphene sheets (GSs) are separated from each other and fixed, thereby preventing agglomeration. Up to now, several strategies to prepare the 3D graphene have been developed, the typical ones include liquid self-assembly with[14] and without[15,16] templates, template-assisted chemical vapor deposition (CVD),[17] gas-assisted "cutting-thin,"[18,19] and self-propagating.[20] The pore size of the reported 3D graphene generally ranges from several to hundreds of micrometers and the electrical conductivity as high as 1000–1204 S m^{-1} has been achieved.[14,17] Although much progress has been made along this route, currently, the 3D graphene still suffers from the problems of too large pore size, low electrical conductivity, and less exposure of the edges. Therefore, further efforts are needed to improve the network structure and thus the properties of the 3D graphene.

Electrospinning is a simple and scalable method producing polymer-based continuous nanofibers in the form of large area membranes. Carbon nanofibers (CNFs) derived from the electrospun polymer nanofibers are intrinsically resistant to agglomeration due to the continuous fiber morphology. Few years ago, we have prepared the CNFs with radially grown GSs by carbonizing the electrospun polyacrylonitrile (PAN) nanofibers in NH_3 in conventional tube furnace.[21,22] The radially oriented GSs may arise from the preferential etching of NH_3 on the graphitic layers oriented along circumferential direction during the carbonization process. However, these surface GSs are too small and only several nanometers in height as the process is only carbonization rather than continuous growth. We envisaged that further growth of the surface GSs into large size may generate an ideal graphene structure, 3D graphene fibers (3DGFs), where the GSs are fixed vertically on the CNFs with the edges exposed on the surface, avoiding agglomeration and preserving the active edges.
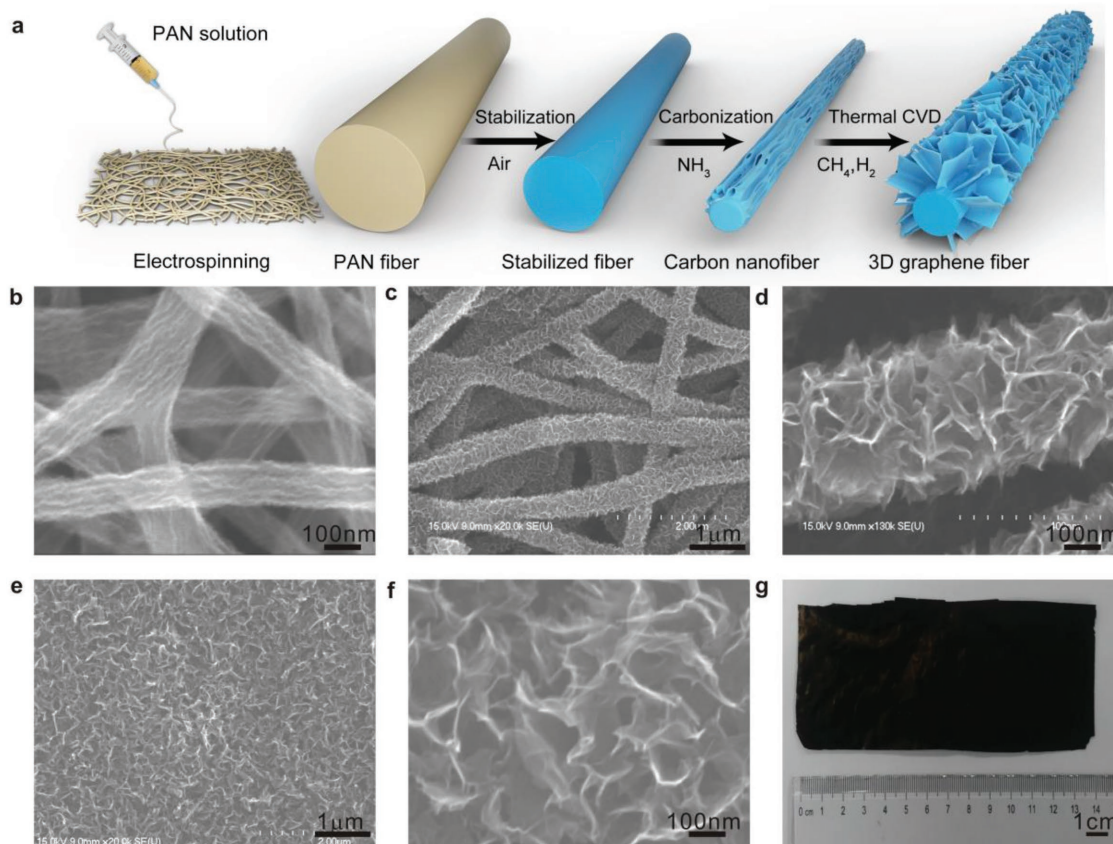
Figure 1. Preparation process and structure of the 3DGFs. a) A schematic illustration of the preparation process. b) A SEM image of the CNFs carbonized in NH_3. c,d) SEM images of the 3DGFs grown for 4 h at CH_4 concentration of 11.1% and 1100 °C. e,f) SEM images of the 3DGFs grown for 10 h at CH_4 concentration of 11.1% and 1100 °C. g) An optical image of the 3DGF membrane.

A reasonable idea to realize the continuous growth of the surface GSs is to introduce carbon-containing gases during or after the carbonization process. However, we noticed that thus far vertical growth of the GSs remains challenging for thermal CVD. The thermal CVD has been widely used to grow high-quality or monocrystal graphene on different substrates such as Cu foil,[23] nickel film,[24] and Si/SiO$_x$ wafer.[25] For these cases, the graphene is grown flat on the substrates. Up to now, most of the successful experiments growing vertical GSs were accomplished by plasma CVD,[26–28] which may be caused by the sheath potential and ion bombardment.

Nonetheless, we expected that vertical growth of the GSs on the CNFs by thermal CVD is possible using the preformed graphene structure as the active nucleation sites or crystal seeds for epitaxy. Finally, we succeeded in growing the vertical GSs by thermal CVD and thus obtaining the 3DGFs. In particular, after long time growth the GSs on different CNFs interconnect and merge with each other, forming a unique porous bulk solid of GSs.

The preparation steps include electrospinning of the PAN nanofibers, stabilization in air, carbonization in NH_3, and growth of the GSs in the mixture of CH_4 and H_2 by thermal CVD (**Figure 1**a). Conventionally, the carbonization process is carried out in protective atmosphere of Ar or N_2. Here, application of NH_3 during the carbonization is for forming graphene structure on the obtained CNFs. It is observed that many clear

streaks form on the CNFs after carbonization in NH_3, corresponding to the small radially grown GSs (Figure 1b).[21,22] This is in sharp contrast to the CNFs carbonized in inert atmosphere, which possess smooth surface (Figure S1, Supporting Information).[29] Temperature plays an important role in the formation of the graphene structure and higher temperature is favorable. In the temperature range of 1000–1100 °C the graphene structure develops well. At too low temperature no graphene structure appears and at too high temperature little products can be obtained due to the strong etching effect of NH_3.[21,22] Simultaneously, the diameter of the CNFs can be reduced effectively due to the etching effect of NH_3, which decreases with increasing the temperature and duration time. In this work, the CNFs were carbonized at 1100 °C for 2 h, leading to an average diameter about 100 nm (Figure 1b).

After finishing carbonization the GSs growth process was in situ initiated by shutting off NH_3 flow and introducing CH_4/H_2 gases without switching off the power source. Figure 1c,d shows the scanning electron microscopy (SEM) images of the sample grown for 4 h at the CH_4 concentration (C_m) of 11.1%. As expected, the GSs grew out vertically on the CNFs without using any catalysts and templates. The fibers exhibit a fluffy appearance and average diameter about 490 nm. Subtracting the diameter of the original CNF substrates, the height of the GSs is about 195 nm. These vertical GSs show a bending and

**ADVANCED
SCIENCE NEWS**

www.advancedsciencenews.com

**ADVANCED
MATERIALS**

www.advmat.de

crumpling morphology with the edges exposed on the surface, which interconnect to form porous structure. The pore size (interspace between the GSs) ranges from 20 to 100 nm, which are well below those of the widely reported 3D graphene. The dependence of the structure and growth rate of the 3DGFs on the growth time was investigated by growing the GSs for 1–35 h. It is found that only after 1 h well-developed GSs can be observed (Figures S2 and S3, Supporting Information). With increasing growth time the density of the GSs and diameter of the 3DGFs increase remarkably (Figures S2–S4, Supporting Information). When increasing the growth time from 1 to 4 h the average diameter of the 3DGFs increases from 138 to 490 nm (Figure S4, Supporting Information). Interestingly, when prolonging the growth time to 10 h, the GSs on different CNFs meet and merge each other and fill all the space between the CNFs, forming a unique porous bulk solids of the GSs (Figure 1e,f). The surface of the 3DGF membranes is uniform, flat, and porous with no larger voids. The morphology of the GSs and porous structure are about similar to those on the individual CNFs. This means that the GSs grow upward uniformly and continuously after the GSs on the different CNFs meet and fill the interfiber space.

In order to further explore the time-dependent structure evolution of the GSs we extended the growth time to 35 h. For this sample the surface are still interconnected GSs (Figure S5, Supporting Information). But the GSs look denser and thicker and the unidirectionality degrades. On this sample, we observed a fiber protruding from the surface as thick as 6 µm, for which both the inner and surface part are radially oriented GSs (Figure S5, Supporting Information). Besides time, the growth of the GSs is also dependent on the temperature and C_m. The growth rate, density, and thickness of the GSs all increase with increasing the temperature and C_m. The temperature and C_m are strongly interactive, and at higher temperature the appropriate C_m range for the GS growth shifts down, which may be due to the enhanced decomposition of CH_4 at high temperature. In this work, the growth temperature from 1000 to 1300 °C was investigated, which indicates that the GSs start to grow from 1050 °C at the C_m of 11.1%. We here focused on the temperature of 1100 °C by balancing the materials structure and growth rate. The appropriate C_m range at 1100 °C is 5–20%, beyond the upper limit only continuous overcoatings form rather the GSs (Figure S6, Supporting Information).

The 3DGFs were prepared in the form of membranes. Even for a small tube furnace (50 mm in diameter) large area 3DGFs membranes can be prepared. Shown in Figure 1f is a piece of the 3DGFs membrane with a size of 137×66 mm^2. The present 3DGFs membranes possess excellent flexibility and resilience. Even bending over 90° and percussing for many times the membrane is intact (Figure S7 and Movie S1, Supporting Information). This excellent flexibility and resilience may be due to the ultrathin diameter of the core CNFs. During application the strength could be further strengthened by supporting on a sticking tap (Figure S7 and Movie S2, Supporting Information) or preparing into 3DGFs/polymer composite membranes (Figure S7 and Movie S3, Supporting Information). It can be seen that the present 3DGFs membrane is strong enough for device application.

We also endeavored to find measures to increase the growth rate of the GSs. In principle, the growth rate of the GSs should be strongly dependent on the dissociation rate of CH_4. We have found that the growth rate of the GSs is higher at higher temperature, which should be caused by the higher dissociation rate of CH_4. We expected that the growth rate of the GSs may be increased by promoting the dissociation of CH_4. In a previous report, copper has been used to enhance the dissociation of CH_4 due to its catalyzing effect, and thus inducing formation of bilayer Bernal graphene.[30] Inspired by this work, we put a block of foam copper before the sample in the upstream position to enhance the CH_4 dissociation during the CVD growth of the GSs (Figure S8, Supporting Information). We delightedly observed that the growth rate of the GSs could be greatly increased by this measure. Only after 10 min well-developed 3DGFs can be obtained (Figure S9, Supporting Information). For the sample grown for 1 h the fiber diameter reached about 570 nm (Figure S9, Supporting Information). Judging from the diameter the growth rate of the GSs is over four times higher when using the copper catalyst than that without using catalyst. Copper element was not detected in the 3DGFs membrane by energy dispersive X-ray spectroscopy (Figure S10, Supporting Information), indicating that the application of the copper catalyst does not bring contaminants to the sample.

Cross-sectional SEM images can give further structural understanding on the 3DGFs. **Figure 2**a–c shows the cross-sectional SEM images of the 3DGFs grown at 1100 °C and C_m of 16.7% for 4 h. It is observed that the GSs grew uniformly on all the CNFs, even for those in the interior (Figure 2b). The average diameter of this sample is about 760 nm, giving an average height of the GSs about 330 nm. The structure of the 3DGFs can be more clearly observed from the cross-section images of a single fiber (Figure 2c). This 3DGF is about 850 nm and the central CNF is about 100 nm (the area with granular morphology), meaning a height about 375 nm for the GSs. The growth rate is higher than that at the C_m of 11.1%. For the 3DGFs grown for 10 h almost no voids are found on the cross-section, indicating that all the interfiber space is filled with the GSs (Figure 2d). Many GSs can be observed both in interior (Figure 2e) and near the surface (Figure 2f). For the 3DGF membrane grown for 35 h the GSs can also be observed both in the interior and surface area. But some sheets became much thicker and larger (Figure S11, Supporting Information).

Transmission electron microscopy (TEM) images shown in **Figure 3**a,b indicate that the GSs grow on all the CNFs uniformly and densely with the fiber diameter about similar to that measured by the SEM images (Figure 1c). The GSs become thinner with approaching the edges, exhibiting a tapered shape. The high-resolution TEM images clearly demonstrate the edge structure of the GSs, e.g., with approaching the edges the thickness decreases from three to one atomic layer (Figure 3c). The interlayer spacing is close to 0.33 nm, consistent with that of the reported GSs.[24] The inner part of the GSs is generally several to more than ten atomic layers in thickness. Numerous images reveal that most of the GSs are one or two atomic layers in thickness in the edge area (Figure 3c,d). The tapered shape seems to be a common feature of the CVD grown nanosheets both for carbon[31] and boron nitride.[32] The formation of the tapered structure may be related to the growth mechanism of
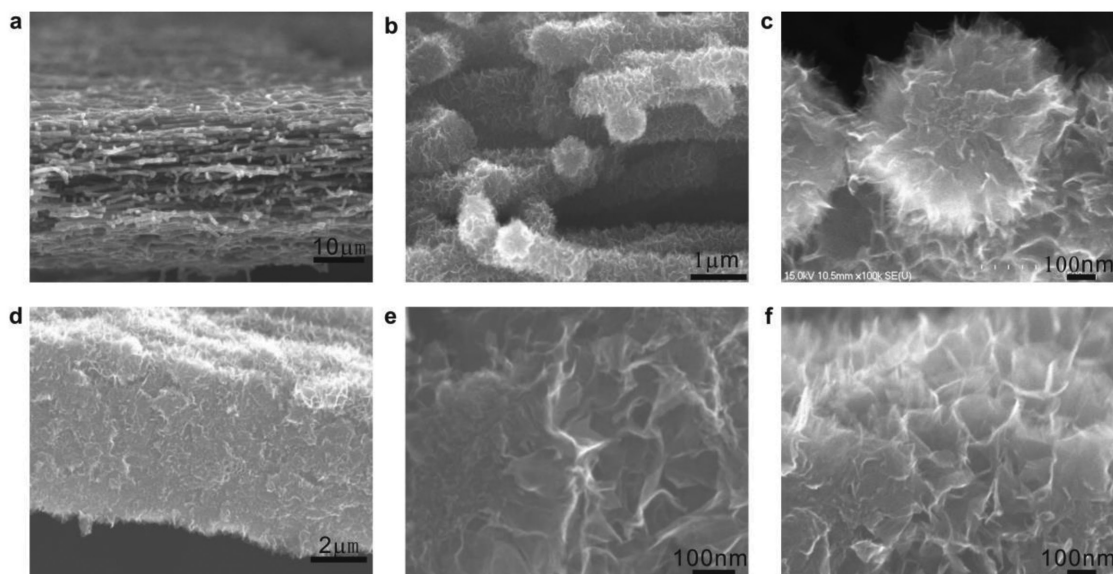
Figure 2. Cross-sectional SEM images of the 3DGFs grown at different conditions. a–c) Growth time 4 h, CH_4 concentration 16.7%. d–f) Growth time 10 h, CH_4 concentration 11.1%. Images (e) and (f) were taken from the interior and surface part of the cross section shown in image (d), respectively.

the GSs such as nucleus structure and etching atmosphere, which needs to be further investigated deeply. From Figure 4c it is noted that the single layer edges may not scroll due to the supporting force from adjacent scrolled edges. Selected area electron diffraction (SAED) pattern measured from the GSs comprises four concentric rings, well corresponding to the (002), (100), (102), and (110) planes of the graphitic structure (Figure S12, Supporting Information), respectively. The ring-shaped SAED pattern is typical of polycrystalline materials.[33] On the (002) ring scattered diffraction spots can be vaguely discerned, indicating that the SAED pattern is from several GSs. The dependence of the thickness of the GSs on the growth time was further investigated by TEM. It is found that with increasing the growth time the edge thickness of the GSs is stable at one to two atomic layers while the thickness of the inner part increases gradually (Figure S3, Supporting Information). As shown in Figure 3e, with increasing the growth time from 1 to 35 h the thickness range of the GSs in the inner part increases from 5–14 to 8–48 atomic layers.

Both the CNFs before growing the GSs and the 3DGFs were characterized by X-ray diffraction (XRD) (Figure 3f). The XRD pattern of the CNFs shows a broad peak centered at 22.5°, corresponding to the (002) reflection of the graphitic structure with a d-spacing about 0.395 nm. The broad shape and big d-spacing arise from the highly defective structure of the CNFs derived from polymer pyrolysis and formation of the surface graphene structure. In our previous work it was found that the d-spacing increases with increasing the carbonization temperature,[22] which conflicts the common sense that the d-spacing should be smaller at higher temperature. We ascribed this phenomenon to the formation of the graphene structure at higher temperature. The (002) peak of the 3DGFs upshifts to about 25° (corresponding to a d-spacing of 0.356 nm) with the intensity and d-spacing decreased comparing with the CNFs. The decrease of the d-spacing is because the CVD grown GSs is better crystallized than the carbonized CNFs while the decrease in intensity

is due to the presence of the GSs. Discontinuous arrangement and less stacking layers for the GSs result in the decrease of the (002) peak intensity. The measured d-spacing of 0.356 nm for the 3DGFs is larger than the theoretical value of graphite, which is because the (002) peak is from the combination of the highly defective CNFs and the well crystallized GSs. The inter-layer spacing measured from the XRD pattern is consistent the TEM results. This peak is typical of the graphene structure and similar to the graphene papers and hydrogels derived from graphene oxide in shape and position.[34,35]

Raman spectra can provide more specific information on the graphene structure. As shown in Figure 3g, obvious 2D peaks appear on the spectra of the 3DGFs grown for different times. The intensity of the 2D peak increases with the growth time and the 3DGFs grown for longer time exhibit very strong 2D peaks. The I_G/I_{2D} ratio decreases with the growth time and reaches 0.88 at the growth time of 10 h (Figure S13, Supporting Information). Appearance of the intensive 2D peak with small I_G/I_{2D} ratio is indicative of the structure of single or few layered graphene, where the I_G/I_{2D} ratios of 0.18, 0.35, and 1.3 correspond to one, two, and three-layered structure,[36,37] respectively. For the present GSs, the edges are one to two layered while the inner parts away from the edges are multilayered as indicated by the TEM, which all contribute to the G peak, leading to the overestimation of the I_G/I_{2D} ratio relative to the edge areas. The present I_G/I_{2D} ratios confirm that the GSs are one to two layered at the edge areas, consistent with the TEM results. The higher I_G/I_{2D} ratio at shorter growth time is caused by the lower density of the GSs (Figures S2 and S3, Supporting Information), where more information is from the core CNFs. Furthermore, with prolonging growth time the I_G/I_D ratio increases initially and then decrease after 3 h (Figure S13, Supporting Information). This is because the CVD grown GSs have higher crystallinity than the PAN-pyrolyzed CNFs. With increasing the growth time the amount of the GSs increases, resulting in the increase of the I_G/I_D ratio. Simultaneously, more graphene
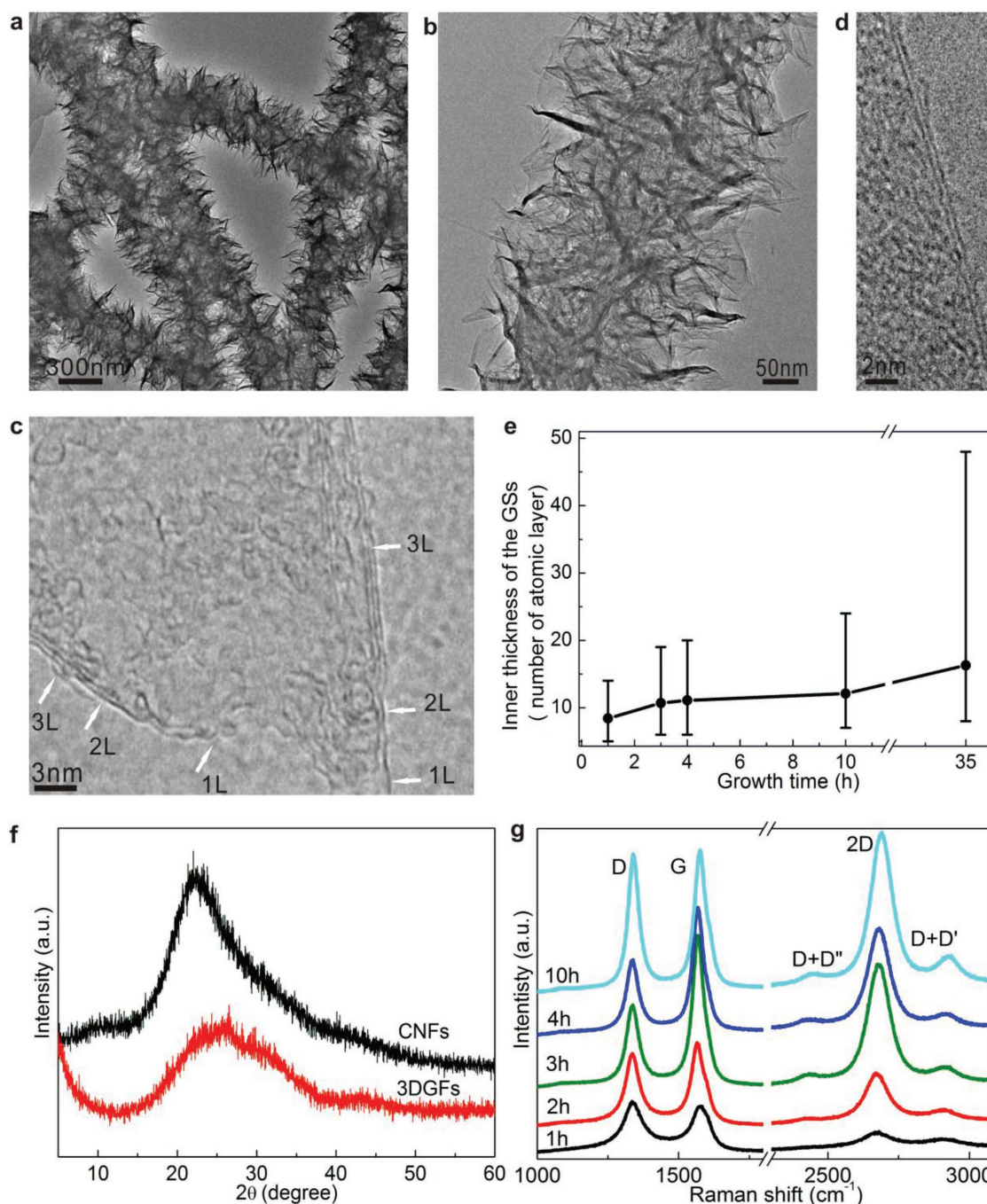
Figure 3. TEM, XRD, and Raman characterization of 3DGFs grown at CH_4 concentration of 11.1%. a,b) TEM images of the 3DGFs grown for 4 h. c,d) Edge structure of the GSs grown for 4 h. e) Thickness of the GSs in the inner parts of the 3DGFs grown for different time. f) XRD patterns of the original CNFs and 3DGFs grown for 4 h. g) Raman spectra of the 3DGFs grown for different times.

edges are concentrated on the surface, which increase the D peak intensity as the edges are highly defective.[36,37] Therefore, after longer time growth the I_G/I_D ratio decreases instead due to more contribution from the edge structure.

As expected, the GSs were vertically grown on the CNFs successfully by the simple and easily scalable thermal CVD. We considered that the unique graphene structure of the NH_3 etched CNFs (as the substrates) and appropriate etching

atmosphere caused by H_2 account for the vertical growth of the GSs. The preformed graphene structure on the CNFs may provide favorable nucleation sites or epitaxial seeds for the vertical growth of the GSs. Unfortunately, we have no way to determine whether the vertical growth of the GSs is epitaxy or not currently. We have also tried to grow the vertical GSs on the CNFs carbonized in Ar with smooth surface, but only particles were obtained. Etching atmosphere is a similarly important
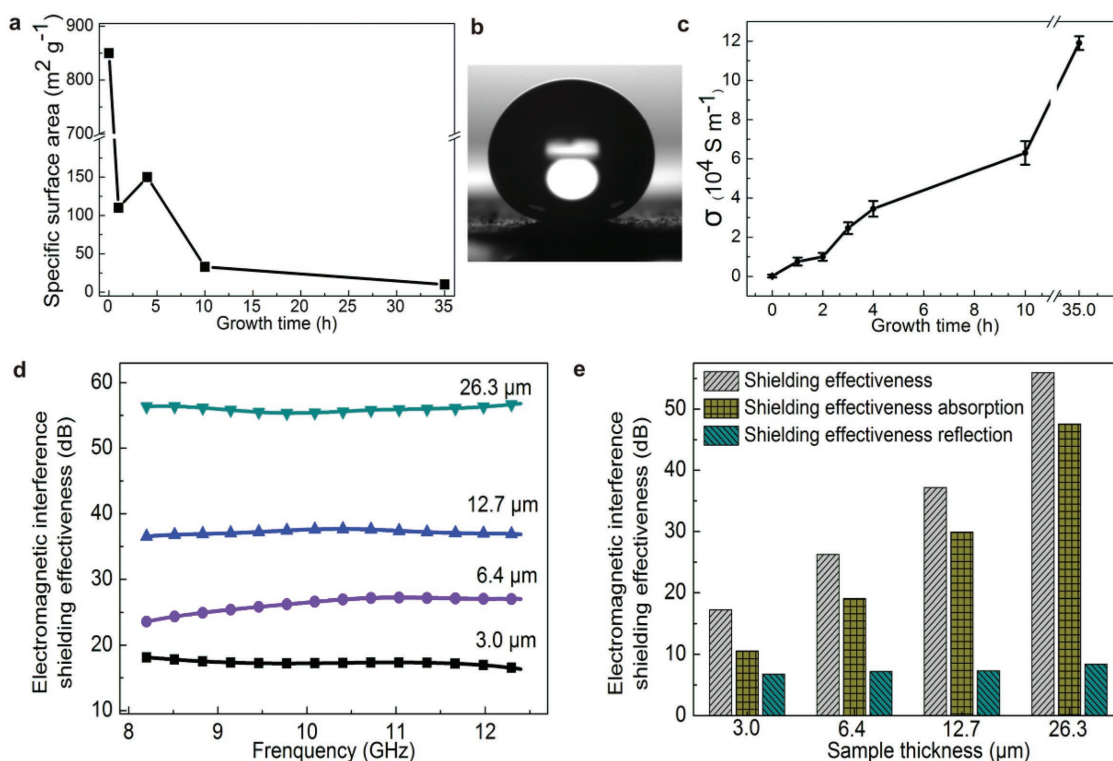
**ADVANCED
SCIENCE NEWS**

www.advancedsciencenews.com

**ADVANCED
MATERIALS**

www.advmat.de

Figure 4. Specific surface area, wetting behavior, electrical conductivity, and electromagnetic interference shielding effectiveness of the 3DGFs grown at CH_4 concentration of 11.1%. a) Specific surface area of the 3DGFs grown for different time. b) An optical image of the water droplet on the 3DGF membrane grown for 10 h. c) Electrical conductivity (σ) of the 3DGFs grown for different times. d) Electromagnetic interference shielding effectiveness of the 3DGF membranes at different thickness. e) Average shielding effectiveness, shielding effectiveness absorption, and shielding effectiveness reflection of the 3DGF membranes at different thickness.

factor to ensure the vertical growth of the GSs, which inhibits the out-of-plane nucleation and growth of the graphitic crystals and promotes formation of the sheet shape. Here H_2 acts as the etchant due to its high reactivity on graphitic carbon. The etching effect increases with increasing the temperature and H_2 concentration. All the experimental results support the present speculation as exemplified by the phenomena that only smooth overcoatings can be obtained at too high CH_4 concentration and in the mixture of Ar/CH_4 (Figures S6 and S14, Supporting Information).

As a basic property and structural feature SSA was measured for the different samples (**Figure 4**a and Figure S15, Supporting Information). The original CNFs possess a high SSA of 850 $m^2\ g^{-1}$. This is because the polymer-derived carbon is highly defective due to NH_3 etching, generating many micropores. However, after growing the GSs for 1 h the SSA decreases sharply to 110 $m^2\ g^{-1}$. This should be because the defective structure, mainly the micropores, of the CNFs is covered during the CVD process. Interestingly, the SSA increases back to 150 $m^2\ g^{-1}$ after growing for 4 h. This increase is caused by the amount increase of the GSs. After growing for 10 and 35 h, the SSA decreases sharply to 34 and 7 $m^2\ g^{-1}$, respectively. These low SSA values suggest that the GSs may become thick and form closed pores after long time growth. This is consistent with the structure evolution of the 3DGFs observed above.

Surface wetting property is also a basic property and important for many applications such as water-resistant, anti-icing,

corrosion resistant, self-cleaning, and adsorption and segregation.[38–41] The superhydrophobicity has been considerably investigated for the conventional graphene materials for extending their application. In previous reports, the seuperhydrophobicity was engendered mainly following two routes, i.e., generating micro/nanoroughness and combining surface roughness with modification using low surface energy chemicals, such as coating the graphene sheets on melamine sponge,[40] crumpling graphene films,[42] generating microscale grating-like structures by laser ablation,[41] laser-induced formation of graphene films in Ar or H_2,[43] and modifying the porous graphene with low surface energy chemicals.[44–47] It is noted that in most reports surface modification is needed to obtain superhydrophobicity for the graphene materials mainly due to the difficulty in generating appropriate porous structure, which introduces impurity and may degrade the intrinsic property of the graphene materials. As to the vertical GSs prepared by plasma CVD, the superhydrophobicity can only be achieved by growing on micropillared Si substrates and modifying with octadecylamine.[48] Therefore, to further develop novel graphene structure with improved superhydrophobic performance is necessary.

As a novel material, the wetting property was investigated for the 3DGFs. It is found that the wetting property of the 3DGFs toward water is dependent on the growth time and the water contact angle increases with increasing the growth time. For the original CNFs the contact angle is 130° (Figure S16, Supporting Information). For the 3DGFs, the contact angle reaches 153°,

**ADVANCED
SCIENCE NEWS**
www.advancedsciencenews.com

**ADVANCED
MATERIALS**
www.advmat.de

168°, 173°, and 173° after growing for 4, 7, 10, and 35 h (Figure 4b and Figures S16 and S17, Supporting Information), respectively. During measurements, it was found that the water droplets were difficult to be transferred onto the sample surface due to the too great repelling force at smaller droplet volume (<5 µL) (Movie S4, Supporting Information). In this work, the water contact angles were all measured at a larger droplet volume of 5 µL. Judging from the water contact angle, the superhydrophobicity of the present 3DGFs is prominent among the graphene-based materials (Table S1, Supporting Information). The superhydrophobicity results from the combination of the intrinsic hydrophobic nature of the GSs and the nanoscale roughness of the vertical GSs. The smaller contact angle for the CNFs and the 3DGFs at shorter growth time is mainly due to the presence of the larger interfiber space and the lower GS density (Figures S2 and S3, Supporting Information). With increasing the growth time the density of the GSs increases and the interfiber space decreases, resulting in the increase of the contact angle. The contact angles of water solution with different PH values were measured for the sample grown for 10 h, which indicates that the superhydrophobicity can be well retained with the contact angle fluctuating in the range of 165°–173° when the PH value changes in the range of 2–12 (Figure S16, Supporting Information) This suggests that 3DGFs possess excellent corrosion-resistant capability. Meanwhile, the 3DGF membranes are superoleophilic with the contact angle of 8° for oil and near 0° for ethanol (Figure S18, Supporting Information). We also etched the 3DGFs by introducing O_2 gas at 600 °C for 10 min after finishing the growth of the GSs. It is found that the surface of the 3DGFs switches from superhydrophobic to superhydrophilic successfully after heat treatment in O_2 (Figure S19, Supporting Information). It is indicated the 3DGFs possess attractive surface wetting properties adjustable from corrosion-resistant superhydrophobicity, superhydrophilicity, and superoleophilicity, suggesting high potential for different applications.

High electrical conductivity is highly required for many applications of the 3D graphene such as energy storage, catalysis, and sensing. Currently, it is still a serious challenge to achieve high electrical conductivity for the 3D graphene materials due to the weak bonding between the constituent GSs. Xin et al. achieved a high electrical conductivity of 2.21×10^5 S m^{-1} for the graphene fibers after annealing at 2850 °C.[49] Li et al. achieved a high electrical conductivity of 1.3×10^4 S m^{-1} by pressing the graphene powder into a pallet at high pressure.[20] Liu et al. prepared continuous graphene fibers by wet spinning of graphene oxide (GO) solution and graphitization treatment at 3000 °C, achieving a superconductivity after Ca intercalation.[50] However, it is noted that the above high electrical conductivities were achieved based on the solid graphitic structure, where the graphitic layers are stacked and connected densely and continuously. When assembling the graphene sheets into well separated 3D porous structure the electrical conductivity decreases greatly as stated above. As shown in Figure 4c, the electrical conductivity of the 3DGF membranes grown for different times was measured using four-probe method. It is found that the electrical conductivity of the original CNFs is very low (184 S m^{-1}). After growing the GSs the electrical conductivity increases quickly. For the 3DGF membranes grown for 4, 10, and 35 h the electrical conductivity reaches 3.4×10^4, 6.3×10^4, and 1.2×10^5 S m^{-1}, respectively.

The present electrical conductivity is much higher than most of the reported 3D graphene (Table S2, Supporting Information). As the electrical conductivity of the original CNFs is very small the high electrical conductivity of the 3DGFs is mainly contributed by the GSs. High crystallinity and tight interconnecting of the GSs account for the high electrical conductivity of the 3DGFs.

For exploring the application form of this material, we pasted the 3DGFs membrane on a transparent sticking tape (Figure S7, Supporting Information) and prepared 3DGFs/poly(dimethylsiloxane) (PDMS) composite membrane by infiltrating PDMS into the 3DGFs membrane (Figure S7, Supporting Information). For these two forms of the 3DGFs-based composite materials we tested their structure durability by measuring their electrical conductivity during bending. It is observed that their electrical conductivities are stable after bending for many times both for the 3DGFs membranes on the sticking tap (Movie S2, Supporting Information) and the 3DGFs/PDMS composite membrane (Movie S3, Supporting Information). Their electrical conductivity kept stable after bending for 80 times (Figure S20, Supporting Information), showing good stability in structure and property. It is indicated that the 3DGFs can be conveniently handled during application.

Viewing from the nanoscale porous structure (abundant interface), continuously interconnected network, high electrical conductivity, and the materials form of large area membrane the 3DGFs is expected to be suitable for application of electromagnetic interference (EMI) shielding. The EMI has become a serious problem with the rapid increase of electronic devices, which influences safe operation of devices and poses hazards to human health. Recently, high performance EMI shielding materials have attracted intensive attention due to the pressing demands.[51–53] As an excellent EMI shielding material, high effectiveness, light weight, and thinness are the main criteria. The EMI shielding effectiveness (SE) of a material is conventionally defined as the logarithm of the ratio of incoming power (P_I) to transmitted power (P_T) formulated as SE (dB) = $10\log(P_I/P_T)$. But this formula is not enough to reflect the intrinsic shielding property of a material as it does not include any material parameters.

A more realistic formula was proposed by considering the influences of weight and thickness of the shielding materials as following, $SSE_{/t}$ (dB cm^2 g^{-1}) = SE/($d \times t$), where $SSE_{/t}$, d, and t are the specific shielding effectiveness, density (g cm^{-3}), and thickness (cm) of the shielding materials, respectively.[52] We measured the EMI shielding capability of the 3DGFs in X-band frequency range, as shown in Figure 4d,e. The 3DGF membranes used for the EMI shielding measurements were grown for 10 h at the C_m of 11.1% with the thickness about 2.8–3.5 µm and density about 0.93 g cm^{-3}. In order to test the effects of the thickness we stacked several pieces of the 3DGF membranes together for measurements. In Figure 4d,e, the thickness of 3.0, 6.4, 12.7, and 26.3 µm corresponds to one, two, four, and eight pieces of the 3DGF membranes, respectively. As expected, the 3DGF membranes exhibit ultrahigh EMI shielding capability. For the 3DGF membranes with thicknesses of 3.0, 6.4, 12.7, and 26.3 µm the average SE can reach 17, 26, 37, and 56 dB (Figure 4d), corresponding to the $SSE_{/t}$ of 60 932, 43 683, 31 327, and 22 895 dB cm^2 g^{-1}, respectively.

Comparing with the reported carbon-based materials the 3DGF membranes are tens to hundreds times thinner at similar SE (Table S3, Supporting Information). The $SSE_{/t}$ of the 3DGF membranes is much higher than the values reported thus far (Table S3, Supporting Information), indicating the high intrinsic EMI shielding performance of the 3DGFs. Obviously, high SE can be attained easily by using more shielding materials; but this is not acceptable due to the corresponding increase of the device weight and size. The present 3DGFs with ultrahigh $SSE_{/t}$ ensuring high SE at ultrathin thickness and light weight represent a significant progress in the area of EMI shielding after the recent progresses such as graphene foams,[51] MXene ($Ti_3C_2T_x$) (30 830 dB cm^2 g^{-1}),[52] and carbon nanotube/graphene hybrid foams (51 000 dB cm^2 g^{-1}).[53]

In principle, the total SE mainly comprises the contribution of surface reflection (SE_R) and internal absorption (SE_A) with $SE = SE_R + SE_A$. For the present 3DGFs the contribution from the internal absorption dominates (Figure 4e and Figure S21, Supporting Information). The excellent EMI shielding performance of the 3DGFs is obviously resulted from the superior structure mainly the nanoscale porous structure and continuously interconnected network, which generates abundant interface and high electrical conductivity. It is worth noting that the single-layered suspended graphene edges may play important roles in the shielding process as they possess high electrical conductivity and thermal conductivity.[1–3]

Vertical GSs have aroused great interest since their successful growth by plasma CVD.[23,24,33] Many attractive applications have been reported for the vertical GSs such as supercapacitor,[54] Li-ion battery,[55] catalysts,[56] sensors,[57] and composites.[58] However, despite the numerous advantages of the vertical GSs the low production capacity of the plasma-based CVD could not meet the demands of many important applications requiring large size or huge amounts of materials such as the above mentioned supercapacitors, Li-ion battery, and composites, which hinders the practical application of the vertical GSs. Therefore, it is a key step to greatly increase the yields of the GSs for their practical application. In the present work, vertical growth of the GSs has been successfully realized by the simple thermal CVD using our unique technique. As well known, the thermal CVD is capable of large-scale production of materials. The present work removed the main obstacle to the practical application of the vertical GSs. In order to demonstrate the production capability and applicability to different substrates of the present technique, we grew the vertical GSs on different substrates with large size including carbon felt (300 × 100 × 12 mm^3) (Figures S22 and S23, Supporting Information), carbon cloth (300 × 100 × 0.4 mm^3) (Figures S24 and S25, Supporting Information), and graphitic paper (280 × 10 × 0.2 mm^3) (Figure S26, Supporting Information). We first coated a layer of PAN on these substrates and then grew the vertical GSs following the above described procedures. It is demonstrated that the vertical GSs were successfully grown on these large-size substrates uniformly. The present sample size is much larger than the size of several to tens of square centimeters reported for the samples prepared by plasma CVD. Due to the tremendous production capacity, low cost, and simplicity of the industrial thermal CVD reactor, the present technique is of high promise for the practical application of the vertical GSs.

In summary, we have realized vertical growth of the GSs on the CNFs carbonized in NH_3 and thus prepared the 3DGFs in a thermal CVD. Comparing with the previous 3D graphene materials the 3DGFs possess unique structure with fibrous shape, nanoscale pores, and exposed single-layered graphene edges. After long-time growth the GSs fill all the space between the CNFs, forming a unique porous solid composed of interconnected graphene and CNFs. The 3DGFs possess high electrical conductivity up to 1.2×10^5 S m^{-1}, high EMI shielding performance with the $SSE_{/t}$ up to 60 932 dB cm^2 g^{-1}, and adjustable wetting property from superhydrophobicity to superhydrophilicity and superoleophilicity, which are much improved comparing with the existing 3D graphene materials. With the extraordinary comprehensive properties and the easy scalability of the simple thermal CVD the novel 3DGFs are highly promising for many applications such as high-strength and conducting composites, flexible conductors, electromagnetic shielding, energy storage devices, catalysis, and separation and purification. Furthermore, the present strategy can be widely used to grow the vertical GSs on many other substrates by predepositing a polymer overlayer and then carbonizing in NH_3 using the thermal CVD.

Supporting Information

Supporting Information is available from the Wiley Online Library or from the author.

Acknowledgements

Conflict of Interest

The authors declare no conflict of interest.

Keywords

[1] Z. S. Wu, W. Ren, L. Gao, J. Zhao, Z. Chen, B. Liu, D. Tang, B. Yu, C. Jiang, H. M. Cheng, *ACS Nano* **2009**, *3*, 411.

[2] H. Wang, K. Kurata, T. Fukunaga, H. Ago, H. Takamatsu, X. Zhang, T. Ikuta, K. Takahashi, T. Nishiyama, Y. Takata, *J. Appl. Phys.* **2016**, *119*, 244306.

[3] A. A. Balandin, S. Ghosh, W. Bao, I. Calizo, D. Teweldebrhan, F. Miao, C. N. Lau, *Nano Lett.* **2008**, *8*, 902.

[4] K. I. Bolotin, K. J. Sikes, Z. Jiang, M. Klima, G. Fudenberg, J. Hone, P. Kim, H. L. Stormer, *Solid State Commun.* **2008**, *146*, 351.

**ADVANCED
SCIENCE NEWS**

www.advancedsciencenews.com

**ADVANCED
MATERIALS**

www.advmat.de

[5] S. V. Morozov, K. S. Novoselov, M. I. Katsnelson, F. Schedin, D. C. Elias, J. A. Jaszczak, A. K. Geim, *Phys. Rev. Lett.* **2008**, *100*, 016602.

[6] Y. Zhu, S. Murali, W. Cai, X. Li, J. W. Suk, J. R. Potts, R. S. Ruoff, *Adv. Mater.* **2010**, *22*, 3906.

[7] K. S. Novoselov, A. K. Geim, S. V. Morozov, D. Jiang, Y. Zhang, S. V. Dubonos, I. V. Grigorieva, A. A. Firsov, *Science* **2004**, *306*, 666.

[8] E. Yoo, J. Kim, E. Hosono, H. S. Zhou, T. Kudo, I. Honma, *Nano Lett.* **2008**, *8*, 2277.

[9] M. D. Stoller, S. Park, Y. Zhu, J. An, R. S. Ruoff, *Nano Lett.* **2008**, *8*, 3498.

[10] Y. Ma, H. Chang, M. Zhang, Y. Chen, *Adv. Mater.* **2015**, *27*, 5296.

[11] C. Huang, C. Li, G. Shi, *Energy Environ. Sci.* **2012**, *5*, 8848.

[12] H. Kim, Y. Miura, C. W. Macosko, *Chem. Mater.* **2010**, *22*, 3441.

[13] S. H. Song, K. H. Park, B. H. Kim, Y. W. Choi, G. H. Jun, D. J. Lee, B. S. Kong, K. W. Paik, S. Jeon, *Adv. Mater.* **2013**, *25*, 732.

[14] B. G. Choi, M. Yang, W. H. Hong, J. W. Choi, Y. S. Huh, *ACS Nano* **2012**, *6*, 4020.

[15] Y. Xu, K. Sheng, C. Li, G. Shi, *ACS Nano* **2010**, *4*, 4324.

[16] H. Bi, X. Xie, K. Yin, Y. Zhou, S. Wan, L. He, F. Xu, F. Banhart, L. Sun, R. S. Ruoff, *Adv. Funct. Mater.* **2012**, *22*, 4421.

[17] Z. Chen, W. Ren, L. Gao, B. Liu, S. Pei, H. M. Cheng, *Nat. Mater.* **2011**, *10*, 424.

[18] X. Wang, Y. Zhang, C. Zhi, X. Wang, D. Tang, Y. Xu, Q. Weng, X. Jiang, M. Mitome, D. Golberg, Y. Bando, *Nat. Commun.* **2013**, *4*, 2905.

[19] Y. Zhao, S. Huang, M. Xia, S. Rehman, S. Mu, Z. Kou, Z. Zhang, Z. Chen, F. Gao, Y. Hou, *Nano Energy* **2016**, *28*, 346.

[20] C. Li, X. Zhang, K. Wang, X. Sun, G. Liu, J. Li, H. Tian, J. Li, Y. Ma, *Adv. Mater.* **2017**, *29*, 1604690.

[21] Y. Qiu, J. Yu, T. Shi, X. Zhou, X. Bai, J. Y. Huang, *J. Power Sources* **2011**, *196*, 9862.

[22] L. Zhao, Y. Qiu, J. Yu, X. Deng, C. Dai, X. Bai, *Nanoscale* **2013**, *5*, 4902.

[23] P. R. Kidambi, D. Jang, J. C. Idrobo, M. S. Boutilier, L. Wang, J. Kong, R. Karnik, *Adv. Mater.* **2017**, *29*, 1700277.

[24] X. Zang, Q. Zhou, J. Chang, K. S. Teh, M. Wei, A. Zettl, L. Lin, *Adv. Mater. Interfaces* **2017**, *4*, 1600783.

[25] J. Pang, R. G. Mendes, P. S. Wrobel, M. D. Wlodarski, H. Q. Ta, L. Zhao, L. Giebeler, B. Trzebicka, T. Gemming, L. Fu, *ACS Nano* **2017**, *11*, 1946.

[26] M. Zhu, J. Wang, B. C. Holloway, R. A. Outlaw, X. Zhao, K. Hou, V. Shutthanandan, D. M. Manos, *Carbon* **2007**, *45*, 2229.

[27] Y. Wu, P. Qiao, T. Chong, Z. Shen, *Adv. Mater.* **2002**, *14*, 64.

[28] J. Zhao, M. Shaygan, J. R. Eckert, M. Meyyappan, M. H. Rümmeli, *Nano Lett.* **2014**, *14*, 3064.

[29] C. Kim, B. T. N. Ngoc, K. S. Yang, M. Kojima, Y. A. Kim, Y. J. Kim, M. Endo, S. C. Yang, *Adv. Mater.* **2007**, *19*, 2341.

[30] K. Yan, H. Peng, Y. Zhou, H. Li, Z. Liu, *Nano Lett.* **2011**, *11*, 1106.

[31] J. Wang, M. Zhu, R. A. Outlaw, X. Zhao, D. M. Manos, B. C. Holloway, *Carbon* **2004**, *42*, 2867.

[32] J. Yu, L. Qin, Y. Hao, S. Kuang, X. Bai, Y. M. Chong, W. Zhang, E. Wang, *ACS Nano* **2010**, *4*, 414.

[33] A. Bachmatiuk, J. Zhao, S. M. Gorantla, I. G. G. Martinez, J. Wiedermann, C. Lee, J. Eckert, M. H. Rummeli, *Small* **2015**, *11*, 515.

[34] H. Chen, M. B. Müller, K. J. Gilmore, G. G. Wallace, D. Li, *Adv. Mater.* **2008**, *20*, 3557.

[35] H. L. Guo, P. Su, X. Kang, S. K. Ning, *J. Mater. Chem. A* **2013**, *1*, 2248.

[36] A. C. Ferrari, J. C. Meyer, V. Scardaci, C. Casiraghi, M. Lazzeri, F. Mauri, S. Piscanec, D. Jiang, K. S. Novoselov, S. Roth, A. K. Geim, *Phys. Rev. Lett.* **2006**, *97*, 187401.

[37] A. Reina, X. Jia, J. Ho, D. Nezich, H. Son, V. Bulovic, M. S. Dresselhaus, J. Kong, *Nano Lett.* **2009**, *9*, 30.

[38] I. Dzięcielewski, J. Weyher, W. Dzwolak, *Appl. Phys. Lett.* **2013**, *102*, 043704.

[39] J. van de Groep, P. Spinelli, A. Polman, *Nano Lett.* **2015**, *15*, 4223.

[40] D. D. Nguyen, N. H. Tai, S. B. Lee, W. S. Kuo, *Energy Environ. Sci.* **2012**, *5*, 7908.

[41] H. B. Jiang, Y. L. Zhang, D. D. Han, H. Xia, J. Feng, Q. D. Chen, Z. R. Hong, H. B. Sun, *Adv. Funct. Mater.* **2014**, *24*, 4595.

[42] J. Zang, S. Ryu, N. Pugno, Q. Wang, Q. Tu, M. J. Buehler, X. Zhao, *Nat. Mater.* **2013**, *12*, 321.

[43] Y. Li, D. X. Luong, J. Zhang, Y. R. Tarkunde, C. Kittrell, F. Sargunaraj, Y. Ji, C. J. Arnusch, J. M. Tour, *Adv. Mater.* **2017**, *29*, 1700496.

[44] J. Rafiee, M. A. Rafiee, Z. Z. Yu, N. Koratkar, *Adv. Mater.* **2010**, *22*, 2151.

[45] Y. Lin, G. J. Ehlert, C. Bukowsky, H. A. Sodano, *ACS Appl. Mater. Interfaces* **2011**, *3*, 2200.

[46] J. S. Lee, J. C. Yoon, J. H. Jang, *J. Mater. Chem. A* **2013**, *1*, 7312.

[47] E. Singh, Z. Chen, F. Houshmand, W. Ren, Y. Peles, H. M. Cheng, N. Koratkar, *Small* **2013**, *9*, 75.

[48] J. Dong, Z. Yao, T. Yang, L. Jiang, C. Shen, *Sci. Rep.* **2013**, *3*, 1733.

[49] G. Xin, T. Yao, H. Sun, S. M. Scott, D. Shao, G. Wang, J. Lian, *Science* **2015**, *349*, 1083.

[50] Y. Liu, H. Liang, Z. Xu, J. Xi, G. Chen, W. Gao, M. Xue, C. Gao, *ACS Nano* **2017**, *11*, 4301.

[51] Z. Chen, C. Xu, C. Ma, W. Ren, H. M. Cheng, *Adv. Mater.* **2013**, *25*, 1296.

[52] F. Shahzad, M. Alhabeb, C. B. Hatter, B. Anasori, S. M. Hong, C. M. Koo, Y. Gogotsi, *Science* **2016**, *353*, 1137.

[53] Q. Song, F. Ye, X. Yin, W. Li, H. Li, Y. Liu, K. Li, K. Xie, X. Li, Q. Fu, L. Cheng, L. Zhang, B. Wei, *Adv. Mater.* **2017**, *29*, 1701583.

[54] G. Xiong, C. Meng, R. G. Reifenberger, P. P. Irazoqui, T. S. Fisher, *Adv. Energy Mater.* **2014**, *4*, 1300515.

[55] Z. Zhang, C. S. Lee, W. Zhang, *Adv. Energy Mater.* **2017**, *7*, 1700678.

[56] W. Li, Z. Zhang, Y. Tang, H. Bian, T. W. Ng, W. Zhang, C. S. Lee, *Adv. Sci.* **2016**, *3*, 1500276.

[57] N. G. Shang, P. Papakonstantinou, M. McMullan, M. Chu, A. Stamboulis, A. Potenza, S. S. Dhesi, H. Marchetto, *Adv. Funct. Mater.* **2008**, *18*, 3506.

[58] Y. Chi, J. Chu, M. Chen, C. Li, W. Mao, H. Zhang, B. S. Liu, H. Shi, *Appl. Phys. Lett.* **2016**, *108*, 211601.